Science
AAAS

Room-temperature coupling between electrical current and nuclear spins in OLEDs

H. Malissa *et al.*

Science **345**, 1487 (2014);
DOI: 10.1126/science.1255624

Science (print ISSN 0036-8075; online ISSN 1095-9203) is published weekly, except the last week in December, by the American Association for the Advancement of Science, 1200 New York Avenue NW, Washington, DC 20005.

REFERENCES AND NOTES

1. L. D. Landau, E. M. Lifshitz, *Statistical Physics, Part 2* (Pergamon, Oxford, 1980).
2. A. J. Leggett, *Rev. Mod. Phys.* **47**, 331–414 (1975).
3. E. Fradkin, S. A. Kivelson, M. J. Lawler, J. P. Eisenstein, A. P. Mackenzie, *Annu. Rev. Condens. Matter Phys.* **1**, 153–178 (2010).
4. S. A. Kivelson, E. Fradkin, V. J. Emery, *Nature* **393**, 550–553 (1998).
5. I. I. Pomeranchuk, *Sov. Phys. JETP-USSR* **8**, 361 (1959).
6. S. Giorgini, L. P. Pitaevskii, S. Stringari, *Rev. Mod. Phys.* **80**, 1215–1274 (2008).
7. C.-H. Cheng, S.-K. Yip, *Phys. Rev. Lett.* **95**, 070404 (2005).
8. V. Gurarie, L. Radzihovsky, A. V. Andreev, *Phys. Rev. Lett.* **94**, 230403 (2005).
9. M. A. Baranov, M. Dalmonte, G. Pupillo, P. Zoller, *Chem. Rev.* **112**, 5012–5061 (2012).
10. T. Miyakawa, T. Sogo, H. Pu, *Phys. Rev. A* **77**, 061603 (2008).
11. B. M. Fregoso, E. Fradkin, *Phys. Rev. Lett.* **103**, 205301 (2009).
12. B. M. Fregoso, K. Sun, E. Fradkin, B. L. Lev, *New J. Phys.* **11**, 103003 (2009).
13. T. Sogo *et al.*, *New J. Phys.* **11**, 055017 (2009).
14. D. Baillie, P. Blakie, *Phys. Rev. A* **86**, 023605 (2012).
15. F. Wächtler, A. R. Lima, A. Pelster, http://arxiv.org/abs/1311.5100 (2013).
16. C.-K. Chan, C. Wu, W.-C. Lee, S. Das Sarma, *Phys. Rev. A* **81**, 023602 (2010).
17. A. Griesmaier, J. Werner, S. Hensler, J. Stuhler, T. Pfau, *Phys. Rev. Lett.* **94**, 160401 (2005).
18. K.-K. Ni *et al.*, *Science* **322**, 231–235 (2008).
19. M. Lu, N. Q. Burdick, B. L. Lev, *Phys. Rev. Lett.* **108**, 215301 (2012).
20. K. Aikawa *et al.*, *Phys. Rev. Lett.* **112**, 010404 (2014).
21. Materials and methods are available as supplementary materials on *Science* Online.
22. M. H. Anderson, J. R. Ensher, M. R. Matthews, C. E. Wieman, E. A. Cornell, *Science* **269**, 198–201 (1995).
23. K. B. Davis *et al.*, *Phys. Rev. Lett.* **75**, 3969–3973 (1995).
24. I. Bloch, J. Dalibard, W. Zwerger, *Rev. Mod. Phys.* **80**, 885–964 (2008).
25. E. Rosenthal *et al.*, *Nat. Phys.* **10**, 225–232 (2014).
26. M. Babadi, E. Demler, *Phys. Rev. A* **86**, 063638 (2012).
27. Z.-K. Lu, S. Matveenko, G. Shlyapnikov, *Phys. Rev. A* **88**, 033625 (2013).
28. L. You, M. Marinescu, *Phys. Rev. A* **60**, 2324–2329 (1999).
29. M. Baranov, M. Mar'enko, V. Rychkov, G. Shlyapnikov, *Phys. Rev. A* **66**, 013606 (2002).

ACKNOWLEDGMENTS

We are grateful to A. Pelster, M. Ueda, M. Baranov, R. Grimm, T. Pfau, B. L. Lev, and E. Fradkin for fruitful discussions. This work is supported by the Austrian Ministry of Science and Research (BMWF) and the Austrian Science Fund (FWF) through a START grant under project Y479-N20 and by the European Research Council under project 259435. K.A. is supported within the Lise-Meitner program of the FWF.

SUPPLEMENTARY MATERIALS

www.sciencemag.org/content/345/6203/1484/suppl/DC1
Materials and Methods
Fig. S1
References (*30*–*41*)

25 April 2014; accepted 15 August 2014
10.1126/science.1255259

ORGANIC ELECTRONICS

Room-temperature coupling between electrical current and nuclear spins in OLEDs

H. Malissa,[1]* M. Kavand,[1] D. P. Waters,[1] K. J. van Schooten,[1] P. L. Burn,[2] Z. V. Vardeny,[1] B. Saam,[1] J. M. Lupton,[1,3]* C. Boehme[1]*

The effects of external magnetic fields on the electrical conductivity of organic semiconductors have been attributed to hyperfine coupling of the spins of the charge carriers and hydrogen nuclei. We studied this coupling directly by implementation of pulsed electrically detected nuclear magnetic resonance spectroscopy in organic light-emitting diodes (OLEDs). The data revealed a fingerprint of the isotope (protium or deuterium) involved in the coherent spin precession observed in spin-echo envelope modulation. Furthermore, resonant control of the electric current by nuclear spin orientation was achieved with radiofrequency pulses in a double-resonance scheme, implying current control on energy scales one-millionth the magnitude of the thermal energy.

Exceptionally large magnetoresistance effects can be observed at relatively low magnetic fields of a few millitesla in organic semiconductors (*1*). Electron spin resonance (ESR) techniques have provided insight into the microscopic origins of spin-dependent transport in these materials and have pointed to hyperfine interactions as the dominant mechanism. Monitoring the device current during coherent spin excitation (*2*–*7*) has revealed signatures of hyperfine coupling that manifest themselves as a resonance line-broadening mechanism. In addition, in nutation experiments under strong microwave excitation, such coupling becomes apparent through the beating of both individual charge-carrier spins at the first harmonic precession frequency, a signature of spin-1 precession (*3*, *5*). Ultimate verification of the influence of nuclear magnetic moments on electronic transport in these highly disordered material systems can only be made by direct electrical detection of nuclear magnetic resonance (NMR). However, at room temperature and the relevant energy scale of NMR, the magnitude of nuclear-level Zeeman splitting is on the order of 100 neV—a million times smaller than the thermal energy kT. Nevertheless, we succeeded in measuring the influence of individual ensembles of nuclear spin states on device conductivity directly through current-detected electron spin-echo envelope modulation and NMR-induced nuclear spin manipulation.

We used poly[2-methoxy-5-(2′-ethylhexyloxy)-1,4-phenylenevinylene] (MEH-PPV) organic light-emitting diodes (OLEDs) as prototypical device structures for pulsed magnetic resonance (*2*, *3*). Electrons and holes were injected electrically to form weakly bound charge carrier pairs within the polymer film (*8*). These pairs exist in either singlet or triplet configuration and can recombine via an excitonic state or dissociate into free charges. In addition, pairs may undergo intersystem singlet-triplet transitions through either incoherent spin-lattice relaxation, or coherent spin manipulation with microwave pulses under ESR conditions. Because of spin statistics, in thermal equilibrium there is an excess population of electron-hole pairs in the triplet state (*9*). In our pulsed electrically detected magnetic resonance experiments, current changes under constant bias (corresponding to a current of ~100 μA dc) were detected as a function of time after a resonant microwave pulse to reveal transient changes in the pair populations through the underlying spin-dependent transport mechanism. Hahn echo and stimulated echo sequences could then be implemented by a small modification of the pulse sequence and subsequent temporal integration of the differential current (*4*, *10*, *11*). This so-called polaron-pair model of spin-dependent transport is not undisputed (*12*), and other carrier-pair mechanisms (such as bipolaron pair formation) have been discussed as the origin for this spin-dependent process (*13*, *14*). Although our discussion is based on the polaron-pair model, the same arguments apply consistently to any Pauli blockade–based spin-dependent transport process. The interpretation of our results is independent of the microscopic nature of this process—e.g., with regard to the electrical polarity of the involved charge carriers, or signs and magnitudes of electronic rates and rate coefficients.

To explore NMR control of the OLED current, we first had to reliably detect the influence of hyperfine coupling on the carrier-pair spin state. To this end, we applied an electrically detected (*11*, *15*) electron spin-echo envelope modulation (ESEEM) technique (*16*–*18*). Nuclear coupling was observed indirectly through coherent manipulation of the electronic spins precessing in the nuclear hyperfine fields and manifested as a modulation of the current spin-echo amplitude superimposed on the exponentially decaying echo signal. This approach is particularly suitable for studying systems with comparatively weak hyperfine interaction strength and low nuclear precession frequencies (i.e., below 5 MHz in an X-band

[1]Department of Physics and Astronomy, University of Utah, Salt Lake City, UT 84112, USA. [2]Centre for Organic Photonics & Electronics, School of Chemistry and Molecular Biosciences, The University of Queensland, Queensland 4072, Australia. [3]Institut für Experimentelle und Angewandte Physik, Universität Regensburg, 93053 Regensburg, Germany.
***Corresponding author. E-mail: hmalissa@physics.utah.edu (H.M.); john.lupton@ur.de (J.M.L.); boehme@physics.utah.edu (C.B.)**

ESR setup operating at a microwave frequency of 9 to 10 GHz, at a resonant field $B_0 \approx 345$ mT, which corresponds to a g-factor of 2.003); strong excitation fields at low excitation frequencies are difficult to establish owing to technical limitations in many electron-nuclear double resonance setups. We applied this technique to OLED devices with MEH-PPV composed of either hydrogenated or deuterated 2-ethylhexyloxy side groups (*3*), as there is a pronounced difference in the nuclear Larmor frequencies of protium and deuterium (14.5 versus 2.2 MHz, respectively, at 345 mT). To reveal spin beating between electronic and nuclear spins in ESEEM, it is important to work at low B_1 fields (weak microwave intensities) so as to avoid purely electronic spin-beating within the spin-1 charge carrier pair (*3*, *5*).

Figure 1 shows results from current-detected ESEEM spectroscopy of the OLEDs. The temporal transient of the spin-echo decay was measured as the time-integrated change in current (i.e., total change in charge ΔQ) (*4*, *10*, *15*). The echo decays exponentially as expected, but also exhibits a superimposed amplitude modulation (Fig. 1, D and J). This oscillation originates from the dipolar coupling of the carrier-pair spin state and the surrounding nuclear spins. The modulation frequency corresponds to the nuclear Larmor frequency. The charge-carrier pairs are weakly coupled, and under sufficiently weak microwave excitation, only the spin-½ transition is excited (*3*, *5*). Consequently, only nuclear modulations of the electron spin arise (*17*), rather than, e.g., electronic spin-spin interactions. The pronounced difference in echo modulation between hydrogenated and deuterated devices is clearly visible without any data processing. The B_0 dependence of the resonance—i.e., the Zeeman splitting (Fig. 1, E and K)—exhibits an unconventional line shape that originates from the pulse sequence projection method used to detect the echoes (*11*) (Fig. 1B). However, the overall resonance line width is typical for MEH-PPV (*2*).

Because the information on nuclear Larmor precession is encoded as a modulation signal in the raw data, Fourier transformation was used to extract the individual frequency contributions (Fig. 1, F to H and L to N). Two different characteristics are visible in the Fourier spectra: (i) a flat, B_0-independent feature close to 15 MHz that persists far off resonance where the echo amplitude itself is zero; and (ii) a strong signal at 14.5 MHz for hydrogenated and at 2.2 MHz for deuterated devices that follows the same B_0-resonance dependence as the echo amplitude (Fig. 1, E and K). The first feature corresponds to the second harmonic of the Nyquist critical frequency and is thus an artifact of finite sampling. Because data acquisition and processing are carried out in the same way for both devices, this feature is identical in both spectra. The second characteristic, the so-called proton or deuteron matrix line, originates from the nuclear spin precession of the respective isotope. A splitting of the matrix line is not observed. This finding is consistent with weak hyperfine coupling of charge carriers to remote nuclear spins, as would be expected in a disordered system (*16*, *18*). Weak coupling arises as the strength of the dipolar hyperfine interaction scales with r^{-3}, where r is the distance between nuclear and electronic spins. From the absence of nuclear line splitting, we can deduce a minimum distance of 0.3 nm between the charge carriers and nuclei (*18*). Such a separation is consistent with the nature of π-electrons in the polymer (Fig. 1, C and I), where the carriers are localized on the

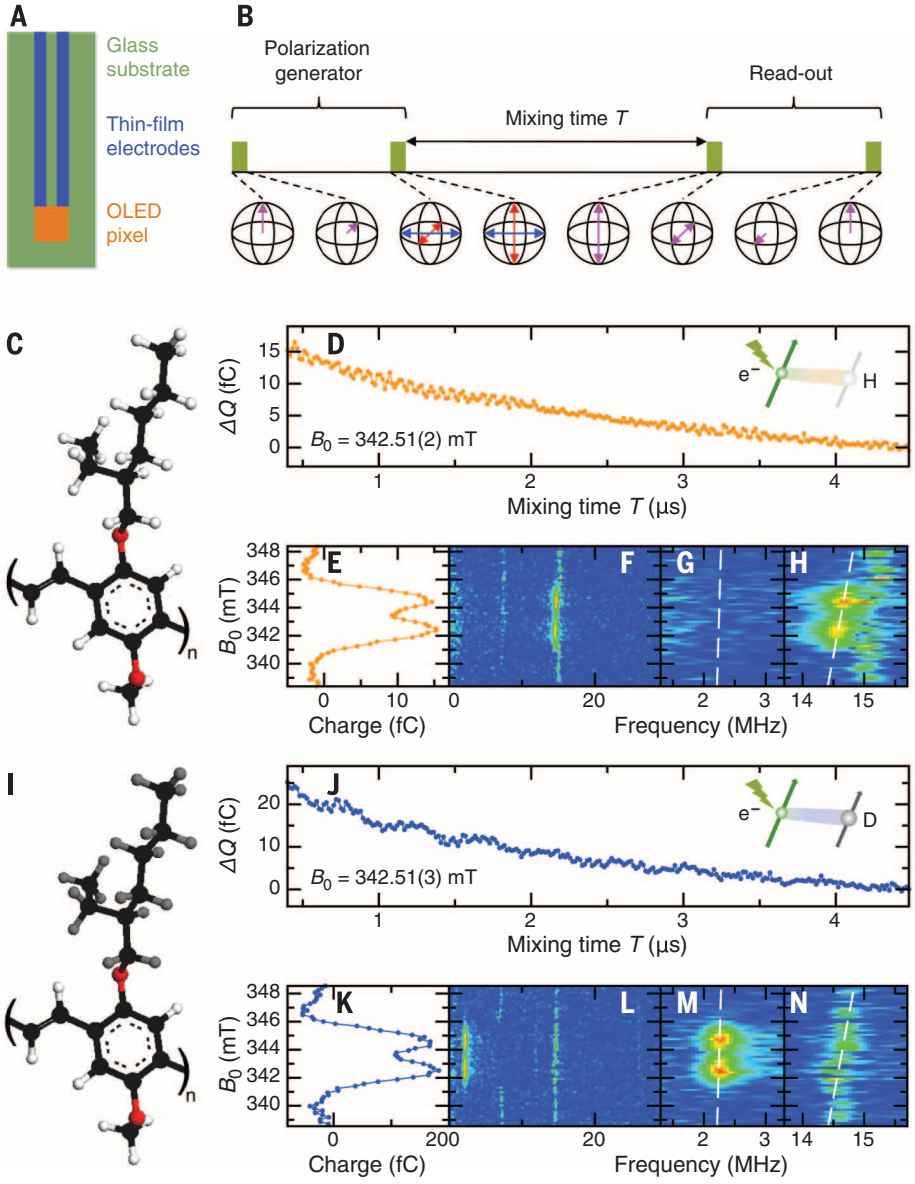

Fig. 1. Isotopic fingerprinting of coherent electronic spin precession in the current of an OLED at room temperature. (**A**) An ITO/PEDOT:PSS/MEH-PPV/Ca/Al OLED pixel was fabricated on an RF/microwave-compatible substrate with thin-film ITO and aluminum contact leads [ITO: indium tin oxide; PEDOT:PSS: poly(3,4-ethylenedioxythiophene):poly(styrene sulfonate)]. (**B**) Scheme for the electrical detection of ESEEM in a stimulated echo sequence. After electronic coherence is generated using a π/2-τ-π/2 ESR pulse sequence, electron and nuclear spins are allowed to mix for a time T before the read-out sequence π/2-τ-π/2 is applied. During T, the electron spins beat with the nuclear spins, imposing a periodic modulation on the spin-echo envelope, which is clearly seen. (**C** and **I**) Chemical structure of the hydrogenated and deuterated MEH-PPV polymers. Black, white, and gray spheres represent carbon, protium, and deuterium. (**D** and **J**) ESEEM signal as a function of mixing time, T. The nuclear resonance signal is contained in the oscillations superimposed on the exponential decay of the current-detected spin echo. The experiments were performed at a microwave frequency of 9.63 GHz. (**E** and **K**) B_0 dependence of the signal. (**F** and **L**) The ESEEM signal after background correction and Fourier transformation for different values of B_0 across the resonance. (**G**, **H**, **M**, and **N**) Magnified views around 2 and 15 MHz, the deuteron and proton matrix lines, respectively. The dashed lines indicate the anticipated frequencies of the proton and deuteron resonances.

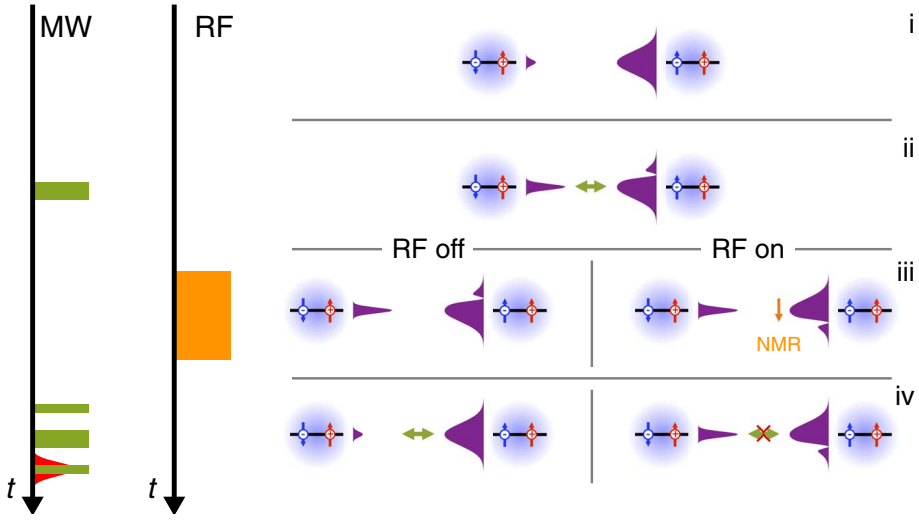

Fig. 2. Microwave (MW) and radiofrequency (RF) pulse sequence and corresponding carrier-pair population distributions for OLED ENDOR spectroscopy. The energetic spread of the populations arises predominantly from hyperfine fields. For simplification, only two of the four singlet and triplet carrier pair states are shown, and the Zeeman splittings between these states are neglected. Transitions between singlet and triplet configurations occur under ESR, leading to a spectral hole in the triplet distribution. Under NMR, the hyperfine field distribution is inverted, blocking resonant refilling of the hole.

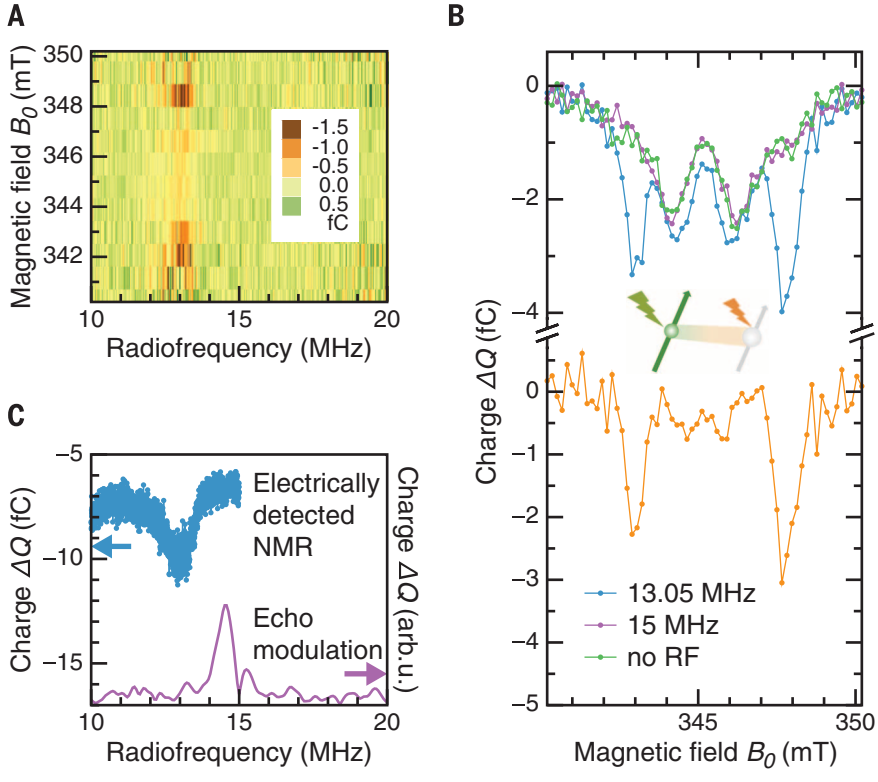

Fig. 3. Direct control of OLED current by nuclear spin transitions. (**A**) Background-corrected Hahn-echo amplitude as a function of RF excitation and B_0 in an ENDOR experiment. Resonance features only appear close to 13 MHz. The experiments were carried out at a microwave frequency of 9.68 GHz. (**B**) Hahn-echo amplitude as a function of B_0 for two different υ_{RF} values (13.05 MHz, blue; and 15 MHz, purple). The spectrum with RF irradiation turned off (green) was used to background-correct the 13.05-MHz data (blue), yielding the pure electrically detected NMR spectrum (orange). (**C**) ENDOR spin-echo amplitude as a function of υ_{RF} at B_0 = 344.1013 mT (blue) compared to the ESEEM spectrum from Fig. 1F (purple).

conjugated backbone and the hydrogenic nuclei are located predominantly in the side groups. The deuterated device does contain a small fraction of protium, but the corresponding matrix line is too weak to be separated clearly from the sampling artifact (Fig. 1N).

Rather than simply correlating a qualitative observable such as magnetoresistance with deuteration (*3*, *6*), these ESEEM experiments constitute direct nuclear magnetic fingerprinting of spin-dependent currents in an organic semiconductor. Given the discrete coupling of electronic spins and device current to nuclear moments, as evidenced by the proton and deuteron matrix lines, it should be possible to coherently transfer spin information between electrons and nuclei as in other solid-state qubit systems such as nitrogen vacancy centers in diamond (*19*) and ^{31}P donor electrons in silicon (*20*, *21*).

To resonantly control the nuclear spin state, we applied high-power radiofrequency (RF) pulses in an electron-nuclear double resonance (ENDOR) configuration that corresponds to a modified Davies-ENDOR sequence (*17*, *21*–*23*). Figure 2 shows the pulse sequence itself with sketches of the relevant carrier-pair spin states. The sequence is rationalized as follows: (i) Before the pulse sequence is applied, the system is in steady state with an excess population of triplet pairs due to spin statistics. The triplet (spin-1) pair distribution is broadened (*5*) by magnetic field interactions (such as Zeeman splitting), whereas the singlet (spin-0) is not. (ii) A microwave π-pulse is applied, which rotates one of the pair partners, turning triplet states into singlets. Only those states in resonance with the pulse are transferred to singlets. This step corresponds to spectral hole burning, because a narrow subensemble of the entire population is depleted. (iii) An RF π-pulse is applied. If this pulse is resonant with the hydrogenic nuclear spin transition (i.e., the pulse energy $E = h\upsilon_{RF}$ corresponds to the Zeeman splitting of the nuclear moments), the nuclear spins are inverted. Consequently, the spectral hole in the triplet pair distribution is inverted (right-hand side). If the RF pulse is nonresonant (or omitted altogether), the nuclear spins remain unaffected (left-hand side). (iv) A modified Hahn-echo pulse sequence π/2-τ-π-τ-π/2-echo (*4*, *10*, *11*) is applied in the microwave channel. This sequence effectively corresponds to a π-pulse and thus again induces transitions between singlet and triplet manifolds. If the RF pulse in step (iii) is nonresonant, singlets are transferred back to triplets, filling the spectral hole in the triplet distribution. The final configuration will then resemble the initial steady-state situation. If, however, the RF excitation is resonant with the nuclear spin transition, the spectral hole in the triplet distribution, detected in the device current, must shift its resonance frequency because the hyperfine interaction strength is modified selectively (the spectral hole is shifted in energy). The resonant transition between singlets and triplets under microwave irradiation (measured by electrically detected magnetic resonance) is then blocked. When the spin-echo amplitude is

subsequently recorded as a function of RF frequency ν_{RF}, the characteristic hydrogen NMR transition frequency should be visible owing to this population quenching, as the relative singlet-triplet pair population controls conductivity (*2*, *14*). It is effectively irrelevant whether a spectral hole or a peak (a population excess) is formed on one of the spin-pair distributions at a specific nuclear resonance energy. The key aspect is that the ESR pulse leads to a departure from equilibrium configuration.

On the peak of the electron spin resonance, when B_0 coincides with the center of the current-detected resonance spectrum (Fig. 1, E and K), a resonant RF excitation will map the inversion of the spectral hole in the triplet population distribution back onto itself. In this case, there is no net change to the nuclear spin population (i.e., the effective hyperfine field), and the current-detected spin-echo amplitude shows no modification. Therefore, NMR control of the current by ENDOR must be conducted slightly off resonance—i.e., at a frequency offset from that observed in current-detected spin precession (ESEEM, Fig. 1), which in turn corresponds to the maximum of the hyperfine field distribution. This argumentation is somewhat simplified and takes neither spin-lattice relaxation (T_1) (*24*) nor electronic processes such as carrier hopping into account (*2*, *4*). The nuclear RF excitation pulses lasted for 10 μs (which corresponds to an RF magnetic field strength at the position of the sample of ~1.2 mT at 240-W RF power). Spin-lattice relaxation together with spectral diffusion will gradually fill up the spectral hole in the triplet distribution while the RF field is applied, thus reducing the overall signal strength. For charge carrier pairs in MEH-PPV, $T_1 \approx 40$ μs at room temperature (*9*), which means that the spectral hole is still pronounced even though the experimental fidelity is limited. In addition, the RF pulse duration places an upper limit on the excitation bandwidth (i.e., the Fourier transform of the pulse), which implies that only a small subset of nuclear spins can be excited resonantly, rather than the entire nuclear spin ensemble.

Figure 3 demonstrates direct control of the OLED current through the nuclear spin of the proton [ENDOR experiments on deuterated devices could not be performed because of the weaker nuclear magnetic moment and several technical limitations relating to the lower resonance frequency (*11*, *17*)]. First, we measured the echo amplitude as a function of B_0 (centered around the current-detected electron-spin resonance) and the nuclear excitation frequency, ν_{RF} (Fig. 3A). The spin-echo–detected B_0-resonance line shape of the electron, which is present both on and off the nuclear resonance (compare to Fig. 1), obscures the ENDOR signal itself. This background was removed by subtracting the off-resonant B_0-dependent signal from the echo amplitude in the absence of RF excitation. The most pronounced features in the two-dimensional ENDOR spectra appear at a nuclear excitation frequency of ~13 MHz and are symmetrical around this resonance with respect to B_0. With these features identified, we performed current-detected spin-echo sweeps of B_0 at different fixed values of ν_{RF} (Fig. 3B, upper panel). When ν_{RF} was detuned from resonance (i.e., to 15 MHz, purple curve) or the RF pulse was omitted altogether (green curve), only the echo-detected line shape was visible, analogous to the results in Fig. 1. However, when ν_{RF} was tuned to the resonance determined from Fig. 3A (13.05 MHz), two additional sharp features appeared on either side of the spin-echo–detected resonance spectrum (blue curve), whereas the central spectral feature remained unaffected. The lower panel of Fig. 3B shows the difference between the blue (nuclear resonance) and green (no RF field) lines, revealing the direct effect of nuclear resonant excitation on device current, the effective ENDOR spectrum. The spectrum is consistent with the understanding of the modified Davies-ENDOR experiment described above: No substantial effect is anticipated close to the center of the charge-carrier resonance (see Fig. 2), where the spectral hole in the distribution of hyperfine fields is mapped back onto itself under inversion, resulting in the observed double-dip feature of the spectrum.

The blue curve in Fig. 3C shows a sweep of ν_{RF} across the hydrogen nuclear resonance with B_0 fixed to the higher-field echo-detected ENDOR peak at 348.5 mT (*11*). For comparison, the nuclear resonance spectrum extracted from the Fourier transform of the current-detected spin-echo envelope modulation of an OLED at the same B_0 field (purple curve, data from Fig. 1) is also shown. Both ESEEM and ENDOR spectra are of comparable width but are shifted with respect to each other by 1.5 MHz. The width of the ENDOR spectrum constitutes a measure of inhomogeneous (disorder) broadening of the hyperfine fields. The shift occurs because the proton matrix line cannot be seen in ENDOR experiments owing to the decreased sensitivity to nuclei with weak (i.e., dipolar) hyperfine-field interaction strengths (*16*). This insensitivity of the method arises from the finite excitation bandwidth of the RF pulses (*17*), which does not present a problem in envelope-modulation detection of intrinsic NMR in the absence of RF manipulation, as in ESEEM. In addition, the ESEEM signal is slightly shifted with respect to the nuclear Zeeman frequency. This shift determines the hyperfine-coupling constant of individual nuclei with the charge carriers (*17*), which in this case accounts for ~4 MHz, or an effective magnetic field strength of 0.1 mT, taking into account that the resonance line splits in two. This value is considerably lower than the hyperfine fields that were previously extracted from ESR line-shape analysis (*5*, *6*), as the latter is determined by the net fields of the entire nuclear spin ensemble acting on the charge carriers. In contrast, here we measure the individual contribution of discrete nuclei, which are selected by the spectral hole–burning procedure.

The room-temperature control of OLED conductivity by direct manipulation of nuclear spin states occurs on an energy scale of ~100 neV (the Zeeman splitting of the nuclear spins at $B_0 \approx$ 345 mT), six orders of magnitude below kT, and therefore constitutes an example of highly efficient switching. Although this effect, originating from strong hyperfine interactions, suggests that protons in organic semiconductors could be used for electrically addressable quantum spin information storage, it is limited with regard to carrier recombination. Coherent writing and read-out of information in nuclear spins in organic semiconductors are not immediately possible because the electronic spins recombine too quickly. However, carrier-pair recombination can be controlled effectively by electric fields (*24*), which could provide a route to enhancing coherent spin-storage times.

REFERENCES AND NOTES

1. R. N. Mahato *et al*., *Science* **341**, 257–260 (2013).
2. D. R. McCamey *et al*., *Nat. Mater.* **7**, 723–728 (2008).
3. S.-Y. Lee *et al*., *J. Am. Chem. Soc.* **133**, 2019–2021 (2011).
4. W. J. Baker, T. L. Keevers, J. M. Lupton, D. R. McCamey, C. Boehme, *Phys. Rev. Lett.* **108**, 267601 (2012).
5. D. R. McCamey *et al*., *Phys. Rev. Lett.* **104**, 017601 (2010).
6. T. D. Nguyen *et al*., *Nat. Mater.* **9**, 345–352 (2010).
7. T. D. Nguyen, B. R. Gautam, E. Ehrenfreund, Z. V. Vardeny, *Phys. Rev. Lett.* **105**, 166804 (2010).
8. S. P. Kersten, A. J. Schellekens, B. Koopmans, P. A. Bobbert, *Phys. Rev. Lett.* **106**, 197402 (2011).
9. D. R. McCamey, S.-Y. Lee, S.-Y. Paik, J. M. Lupton, C. Boehme, *Phys. Rev. B* **82**, 125206 (2010).
10. H. Huebl *et al*., *Phys. Rev. Lett.* **100**, 177602 (2008).
11. Materials and methods are available as supplementary materials on *Science* Online.
12. C. Boehme, J. M. Lupton, *Nat. Nanotechnol.* **8**, 612–615 (2013).
13. G. Li, C. H. Kim, P. A. Lane, J. Shinar, *Phys. Rev. B* **69**, 165311 (2004).
14. M. Wohlgenannt, *Phys. Status Solidi RRL* **6**, 229–242 (2012).
15. M. Fehr *et al*., *Phys. Rev. B* **84**, 193202 (2011).
16. W. B. Mims, J. Peisach, J. L. Davis, *J. Chem. Phys.* **66**, 5536–5550 (1977).
17. A. Schweiger, G. Jeschke, *Principles of Pulse Electron Paramagnetic Resonance* (Oxford Univ. Press, New York, 2001).
18. S. A. Dikanov, Y. D. Tsvetkov, *Electron Spin Echo Envelope Modulation (ESEEM) Spectroscopy* (CRC Press, Boca Raton, FL, 1992).
19. P. C. Maurer *et al*., *Science* **336**, 1283–1286 (2012).
20. M. Steger *et al*., *Science* **336**, 1280–1283 (2012).
21. D. R. McCamey, J. Van Tol, G. W. Morley, C. Boehme, *Science* **330**, 1652–1656 (2010).
22. F. Hoehne, L. Dreher, H. Huebl, M. Stutzmann, M. S. Brandt, *Phys. Rev. Lett.* **106**, 187601 (2011).
23. C. E. Fursman, C. Teutloff, R. Bittl, *J. Phys. Chem. B* **106**, 9679–9686 (2002).
24. M. Reufer *et al*., *Nat. Mater.* **4**, 340–346 (2005).

ACKNOWLEDGMENTS

This work was funded by the U.S. Department of Energy, Office of Basic Energy Sciences, Division of Material Sciences and Engineering under Award DESC0000909. We also acknowledge the Utah NSF–Materials Research Science and Engineering Centers program (DMR 1121252) supporting the acquisition and development of the experimental facilities. P.L.B. is a University of Queensland Vice-Chancellor's Senior Research Fellow. We thank J. Yu for preparing the deuterated MEH-PPV.

SUPPLEMENTARY MATERIALS

www.sciencemag.org/content/345/6203/1487/suppl/DC1
Materials and Methods
Figs. S1 to S4
References (*25*, *26*)

5 May 2014; accepted 31 July 2014
10.1126/science.1255624